Deep learning enabled robust wavefront sensing for active beam smoothing with continuous phase modulator

Yamin Zheng [1,2,3], Yifan Zhang [1,2,3], Liquan Guo [1,2,3], Pei Li [1,2,3], Zichao Wang [1,2,3],

Yongchen Zhuang [1,2,3], Shibing Lin [1,2,3], Qiao Xue [4], Deen Wang [4,5], and Lei Huang [1,2,3,*]

[1] *Department of Precision Instrument, Tsinghua University, Beijing 100084, China*

[2] *State Key Laboratory of Precision Space-time Information Sensing Technology, Beijing 100084, China*

[3] *Key Laboratory of Photonic Control Technology (Tsinghua University), Ministry of Education, Beijing 100084, China*

[4] *Research Center of Laser Fusion, CAEP, P.O. Box 919-988, Mianyang 621900, China*

[5] *sduwde@126.com*

[*] *hl@tsinghua.edu.cn*

Abstract In laser systems requiring a flat-top distribution of beam intensity, beam smoothing is a critical technology for enhancing laser energy deposition onto the focal spot. The continuous phase modulator (CPM) is a key component in beam smoothing, as it introduces high-frequency continuous phase modulation across the laser beam profile. However, the presence of the CPM makes it challenging to measure and correct the wavefront aberration of the input laser beam effectively, leading to unwanted beam intensity distribution and bringing difficulty to the design of the CPM. To address this issue, we propose a deep learning enabled robust wavefront sensing (DLWS) method to achieve effective wavefront measurement and active aberration correction, thereby facilitating active

beam smoothing using CPM. The experiment results show that the average wavefront reconstruction error of the DLWS is $0.04\mu m$ in RMS, while the Shack-Hartmann wavefront sensor's reconstruction error is $0.17\mu m$.

Key words: beam smoothing, continuous phase modulator, deep learning, wavefront sensing.

I. INTRODUCTION

Continuous phase modulation (CPM) is extensively employed in laser systems to achieve beam smoothing and generate a flat-top intensity distribution of focal spots, thereby facilitating subsequent applications that necessitate uniform laser focusing on the irradiation target [1–6]. Ensuring the uniformity of laser irradiation on the focal spot represents a critical and formidable technological pursuit. CPM functions as a transmission-type phase modulating device, introducing high-frequency phase distortion into the beam. Under the influence of CPM, the resulting focal spot of the output beam can be transformed into a circular or elliptical shape with evenly distributed intensity, rather than conforming to a Gaussian distribution pattern [7–10]. However, wavefront distortion occurs during beam propagation due to thermal effects, manufacturing errors, or air turbulence. In contrast, the design of the CPM is based on an ideal plane wavefront input. Therefore, when the input beam contains wavefront distortions, the beam smoothing capability of the CPM decreases and the resulting focal spot no longer maintains a uniform intensity distribution, which leads to laser-plasma instabilities in experiments [11–20].

As an effective method to correct wavefront distortion and improve beam quality, adaptive optics (AO) is widely used in laser systems [21–24]. There are two common types of AO systems. The first type is the wavefront sensorless AO system, measuring a specific parameter of the focal

spot as the control target [25–28]. A two-stage wavefront sensorless AO method based on deformable mirror (DM) resolution-matching was proposed [25]. This method firstly uses the encircled energy of the focal spot as the system performance metric, and then uses the fraction of certain intensity as the system performance metric to control the intensity uniformity. The second type of AO systems is the wavefront sensing AO system, measuring the wavefront of the beam as the control target [29,30]. Compared with the wavefront sensorless AO method, the wavefront sensing AO method usually uses direct correction algorithms with quicker convergence speed. However, under the influence of the CPM, the wavefront sensing AO could not be effectively utilized. With the phase modulation effect of the CPM, the output beam contains high frequency phase distortions, and the wavefront sensor could only measure the wavefront that is already modulated by the CPM. Considering that the control target is to correct the wavefront distortion before the CPM instead of the wavefront distortion after the CPM, it is difficult to implement the correction using wavefront sensing AO method. Another obstacle to the use of wavefront sensing AO method in CPM laser system is the difficult wavefront measurement. As a commonly used tool in AO, the Shack-Hartmann wavefront sensor (SHWFS) measures the wavefront by splitting the beam into several sub-apertures and calculating the slopes of local wavefront within each sub-aperture. Nonetheless, under the influence of the CPM, the high frequency phase distortion in the beam causes dispersed focal spot patterns in the SHWFS and the slope calculation goes wrong, resulting in wrong wavefront measurement results.

To improve the accuracy and speed of wavefront reconstruction, the deep learning technique has been adopted in SHWFS [31–33]. A deep learning wavefront sensing approach for the SHWFS was proposed to predict the wavefront directly from sub-aperture images without centroid calculation [31]. A learning-based SHWFS was proposed to obtain Zernike coefficient

amplitudes of aberrations from the raw image input, achieving high-order aberration detection without image segmentation or centroid positioning [32]. Moreover, the learning-based SHWFS was further developed to achieve direct prediction of discrete phase values with high speed and high accuracy [33]. While the deep learning assisted SHWFS could address the accuracy and speed limitations of direct wavefront reconstruction, it remains a challenge to accurately identify and recover the wavefront distortion to be corrected from distorted SH patterns.

A deep learning assisted high robustness wavefront sensing (DLWS) method for active CPM modulation in beam smoothing is proposed. Through the DLWS method, the wavefront before the influence of the CPM could be accurately extracted and recovered from the SH patterns for direct aberration correction. The DLWS firstly measures the spot patterns of the beam through a SHWFS without slope calculation. The spot patterns are input into a slope deblur neural network (SD-Net) to obtain the accurate slopes of the input laser beam. After that, the CPM-unaffected wavefront could be reconstructed using these slopes and the regular AO process could be implemented to correct the wavefront distortion. With the DLWS method, active beam smoothing with CPM could be carried out to achieve desired intensity distribution of the focal spot.

II. PRINCIPLE AND SIMULATION

The CPM functions as a beam smoothing device, generating a specific phase distribution with characteristic dimensions to modulate the phase at high spatial frequency, thereby achieving the desired light intensity distribution. Figure 1 shows the CPM modulation process.
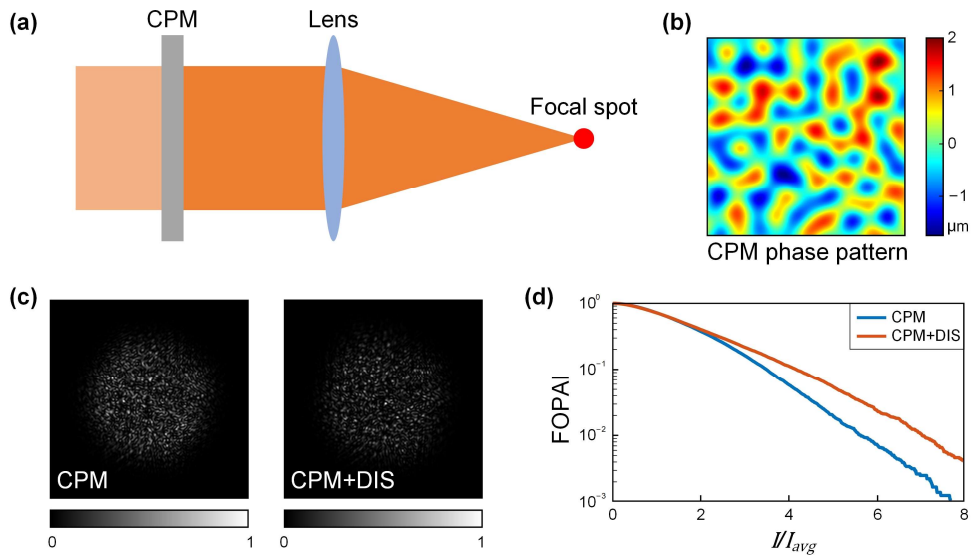
4

Figure 1. CPM modulation in layer systems. (a) CPM optical path. (b) Phase pattern of CPM. (c) Beam profiles with CPM modulation and wavefront distortion (DIS). (d) FOPAI curves with CPM modulation and DIS.

The CPM works at the beam smoothing process in the laser system. The surface shape of the CPM is finely manufactured to introduce continuous phase variations across the laser beam profile, thereby redistributing the laser energy. Figure 1(b) shows the continuous phase variation introduced by the CPM, which redistributes the laser energy profile from a Gaussian form into a flat-top form. Figure 1(c) shows the laser beam profile after the CPM modulation. Before the modulation, the profile follows a Gaussian distribution and the energy is mainly enclosed in the middle area, forming a peak in the center. After the CPM modulation, the profile follows a flap-top distribution, and the energy is evenly distributed around the effective area. Therefore, the uniformity of the laser beam profile is improved. A parameter that is commonly used to assess the uniformity of the focal spot is the fractional power above the intensity (FOPAI). FOPAI of beams before and after the CPM modulation are shown in Figure 1(d). The lower the curve, the better the uniformity. It could be seen that the CPM modulation could effectively improve the uniformity of the laser beam. The CPM could be designed according to system requirements in the specific

5

application. However, to ensure the beam smoothing performance of the CPM, the wavefront distortion of the input laser beam should be effectively corrected.

The wavefront distortion of the input laser beam will cause performance loss of the CPM modulation. Figure 1(c) shows the laser beam profile when the input wavefront contains undesired distortions. The distortions could be introduced by the thermal effect of the lenses, the alignment errors of the optical devices or the air turbulences. Under the circumstance of distorted input laser beam, the CPM modulation could not reach its designed and optimized output. The output laser beam profile's uniformity is not guaranteed. Therefore, in order to maintain the uniformity and stability of the beam profile, active wavefront aberration correction is required.
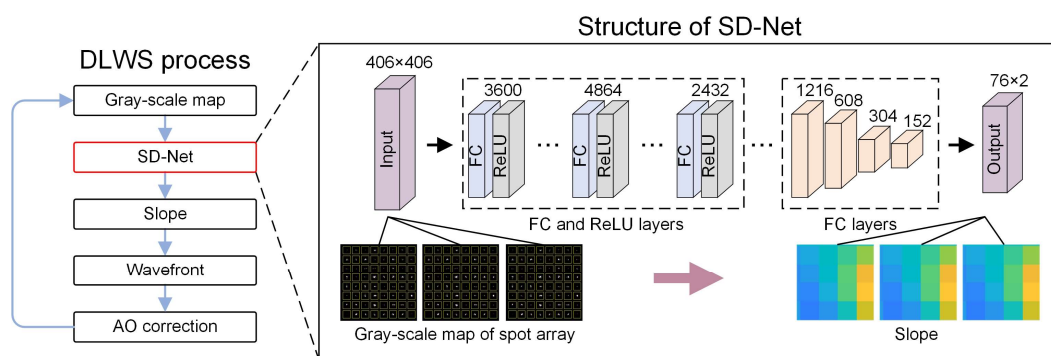

Figure 2. Principle of DLWS and network structure of SD-Net. The input of SD-Net is the raw gray-scale map of the spot array and the output is the slope of each individual sub-aperture.

The DLWS is an effective wavefront sensing method that could measure the wavefront accurately and accomplish wavefront correction towards the right correction direction. The principle of the DLWS is shown in Figure 2. A detector with micro-lens array is used to measure the focal spot array of the input laser beam. The data processing of the DLWS is different from that of the SHWFS. In the DLWS, after the focal spot array is recorded by the detector, the gray-scale map is fed into the slope deblur neural network (SD-Net) to get the local wavefront slope within each sub-aperture. Given that the ground truth slopes are measured by the same SHWFS, the slope information is chosen as the prediction of the SD-Net due to the simplicity of training

6

and calculation. After that, the wavefront could be reconstructed with the accurate slope information by Southwell zonal phase estimation method and the closed-loop correction could be carried out [34]. In order to calculate the full aperture light intensity information without lossy sampling, the fully connected layers are used in the SD-Net. Thresholds are set on the camera in real-time operation to improve the signal-to-noise ratio of the spot array. Due to the concentrated light intensity inside each sub-aperture and the detection threshold of the camera, the weights involved in training loops are distributed sparsely. It should be noted that when the DLWS method is applied to other CPM applications, the structure and scale of the SD-Net should be fine-tuned to achieve directed parameter tuning. While for the SHWFS, the deviation between the measured focal spot array and the array of an ideal input beam is used to calculate the wavefront slopes. The wavefront is reconstructed using these wavefront slopes. However, under the effect of the CPM modulation, the distribution of each focal spot is blurred, which leads to errors in the calculation of centroids and wavefront slopes.

The wavefront measurement and aberration correction performance of the SHWFS under the CPM modulation is investigated in simulation. Figure 3 shows the slope calculation results under the CPM modulation using the DLWS and the SHWFS. The phase variation introduced by the CPM is shown in Figure 1(b). The SHWFS has an 8×8 micro-lens array. Figure 3(a) shows the beam modulation results of the CPM when the input laser beam contains aberrations. After the modulation, the beam profile became more evenly distributed. However, due to the distortion of the input wavefront, the output could not satisfy the CPM designed output and could be improved with AO. Figure 3(b) shows the initial gray-scale maps of the focal spot array measured by the SHWFS after the CPM modulation. From the enlarged picture it could be seen that after the CPM

7

modulation, blur occurs on the focal spots. The distorted focal spots could not reveal the slope of local wavefront accurately. Shown in Figure 3(c) is the wavefront distortion.
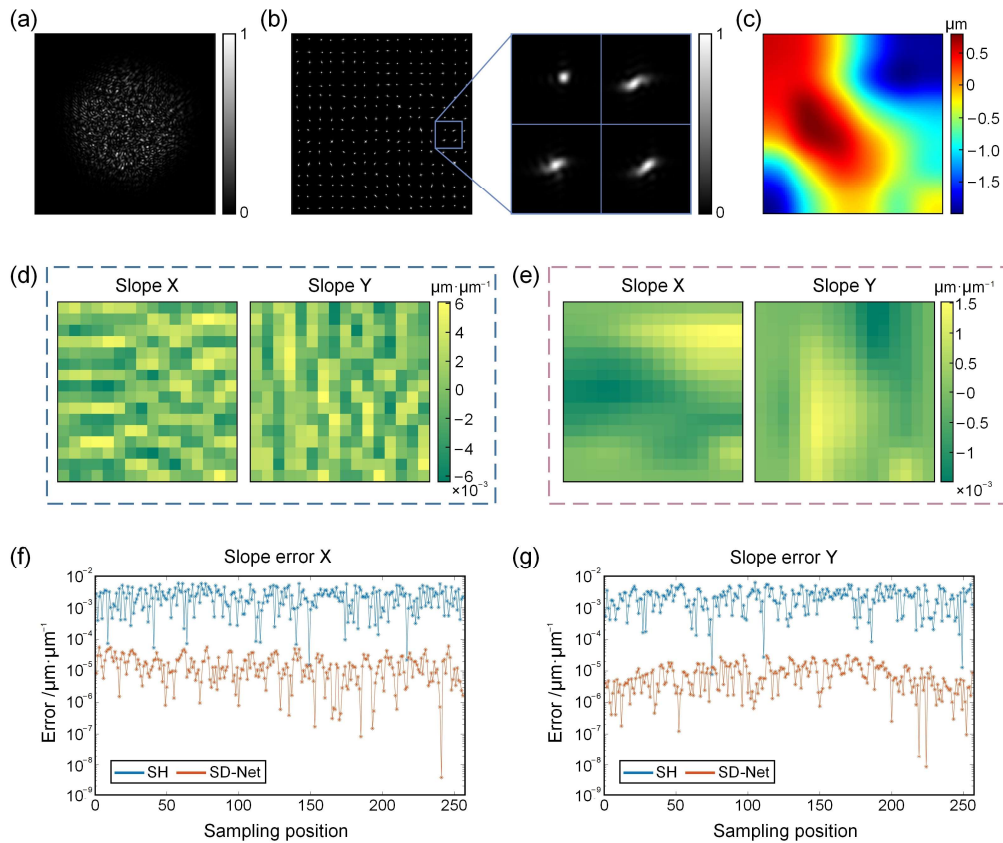

Figure 3. Slope calculation results using DLWS and SHWFS. (a) Beam profile with DIS. (b) Spot array and the enlarged area with DIS.(c) DIS. (d) Slopes calculated by SHWFS. (e) Slopes calculated by DLWS. (f) Slope error in X direction. (g) Slope error in Y direction.

Figure 3(d) and Figure 3(e) show the calculated slopes and wavefront based on the focal spot arrays using SHWFS and DLWS, respectively. It could be seen that the blur causes error in the calculation of wavefront. Figure 3(f) and Figure 3(g) show the slope calculation errors, which are the absolute values of the difference between reconstructed slopes and the ground truth.

In order to improve the uniformity of the output beam profile, the AO should implement correction based on the input beam's aberrations. After correction, the input beam is closer to a plane wave and the CPM modulation achieves better performance. However, considering the

8

modulation of the CPM, during real-time measurement, only the inaccurate CPM-modulated wavefront could be measured, which brings difficulties to AO implementation.

Different from existing approaches to SHWFS reconstruction, the DLWS avoids the slope calculation error by directly recovering slopes using the SD-Net. The DLWS contains three steps. The first step is to get the gray-scale map of each focal spot using a detector with a micro-lens array and a camera, which is the same as the detector used in SHWFS. The second step is to feed the segmented gray-scale map into the SD-Net to get the slopes of local wavefront within each sub-aperture. The third step is to reconstruct the wavefront using the derived slopes. The SD-Net is a neural network trained before the AO implementation. In the training of the SD-Net, the input dataset is the gray-scale map with the CPM modulation and the ground truth dataset is the slope of the wavefront without the CPM modulation. The structure of the SD-Net is flexible. In this simulation and experiment, the SD-Net consists of two sets of cascade neural networks, of which the first set contains three fully connected (FC) layers and three ReLU activation layers, adding nonlinear computing power to the network; The second group contains four fully connected layers, as shown in Figure 2. For each pair of input and output data, the input is a 406×406 matrix of gray-scale map and the output is a 76×2 matrix of slopes in X and Y directions. To generate the dataset suitable for the training, 10000 groups of random laser data before and after the CPM modulation are produced, including wavefront, beam profile and focal spots array measured by the detector. 80% of them are for training and 20% for testing. The loss function is the root-mean-square (RMS) value of the difference between the output data and corresponding ground truth. Figure 3(e) shows the slope calculation result of the DLWS with the same focal spot array after the CPM modulation. The reconstructed wavefront and fitting residue based on it are shown in Figure 4. It could be seen that compared with the SHWFS, the DLWS could reconstruct wavefront with higher accuracy.
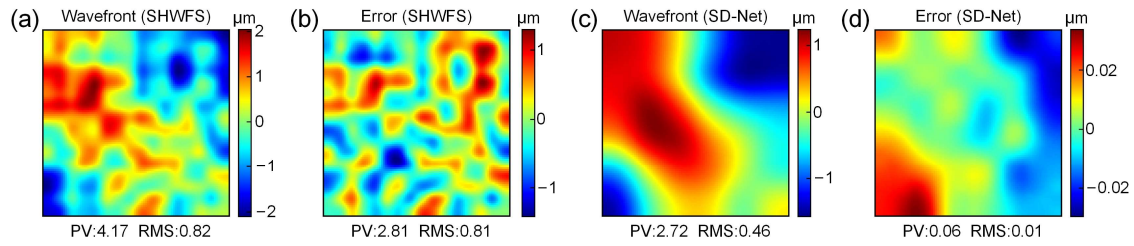
9

Figure 4. Wavefront reconstruction results using DLWS and SHWFS. (a) Wavefront reconstructed by SHWFS. (b) Wavefront reconstruction error of SHWFS. (c) Wavefront reconstructed by DLWS. (d) Wavefront reconstruction error of DLWS.

III. Experiment

The configuration of the experiment and the manufactured CPM is shown in Figure 5. The laser source is a 1053nm laser emitted through fiber. The reflecting mirror (RM) is a plane mirror with good flatness. The CPM manufactured in our lab is shown in the left part of Figure 5. Lenses with different focal lengths are used for beam collimation. A DM is used to implement the wavefront correction and generate different wavefront data for network training. The DM has a 17.5mm pupil diameter and 69 actuators across the whole pupil with a 2.5mm actuator pitch. A detector composed of a charge-coupled-device (CCD) and a micro-lens array is used to measure the gray-scale map of the beam's focal spot array. The CCD has 1000×1000 pixels with a 7.4μm pixel pitch. The MLA has 23×23 sub-apertures with an 8mm focal length. Another CCD is used to measure the laser beam profile with 1384×1360 pixels and a 6.45μm pixel pitch. In the experiment, 18000 groups of random wavefronts are generated by the DM for network training. The training parameters and network structure of the SD-Net in the experiment are the same as in the simulation.
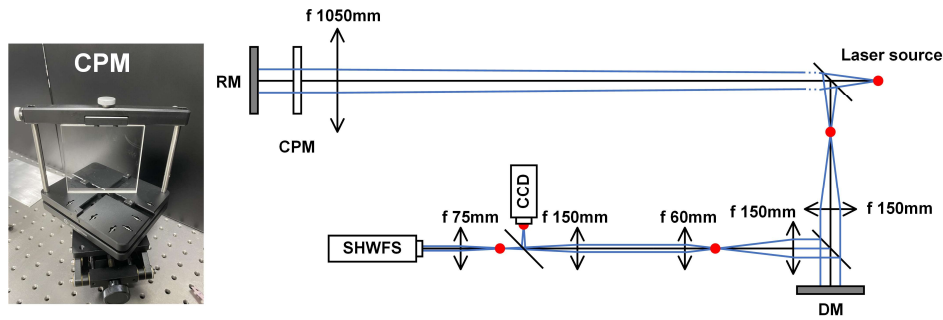
10

Figure 5. Experiment configuration of DLWS. (CPM, continuous phase modulator. RM, reflecting mirror. SHWFS, Shack-Hartmann wavefront sensor. CCD, charge-coupled-device. DM, deformable mirror.)

After the SD-Net is set up, the DLWS could measure the wavefront before the CPM modulation with the modulated laser beam. Figure 6 shows the wavefront measurement results of the DLWS. In order to compare the DLWS and the SHWFS in wavefront measurement accuracy, the gray-scale map measured by the detector is also processed following regular SHWFS calculation principle. Figure 6 shows the spot array captured by the CCD and the wavefront reconstruction errors of the SHWFS and the DLWS. It could be seen that the DLWS wavefront reconstruction accuracy is higher than the SHWFS. The wavefront reconstruction error of the DLWS has a peak-to-valley (PV) value of 0.16μm and an RMS value of 0.08μm. While the error of the SHWFS has a PV value of 0.85μm and an RMS value of 0.43μm.
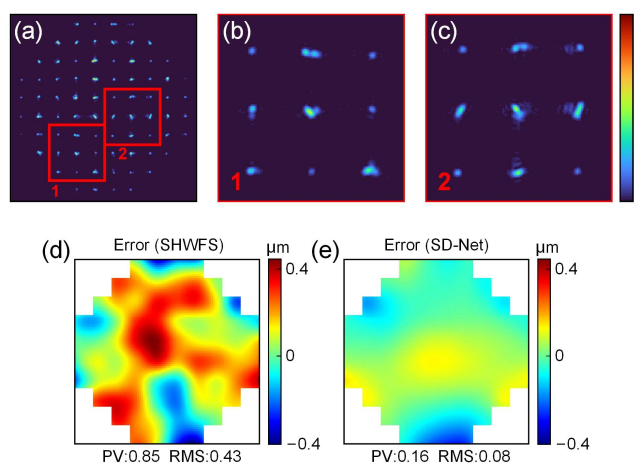

Figure 6. Wavefront results using DLWS and SHWFS in experiment. (a) Spot array. (b)(c) Spots in local sub-apertures. (d) Wavefront reconstruction error of SHWFS. (e) Wavefront reconstruction error of DLWS.

11

More groups of wavefront data are measured by the DLWS and SHWFS as shown in Figure 7. The two charts of curves are the RMS values of the slope calculation error and wavefront error, respectively. The average wavefront reconstruction error of the DLWS is 0.04μm, lower than that of the SHWFS (0.17μm).
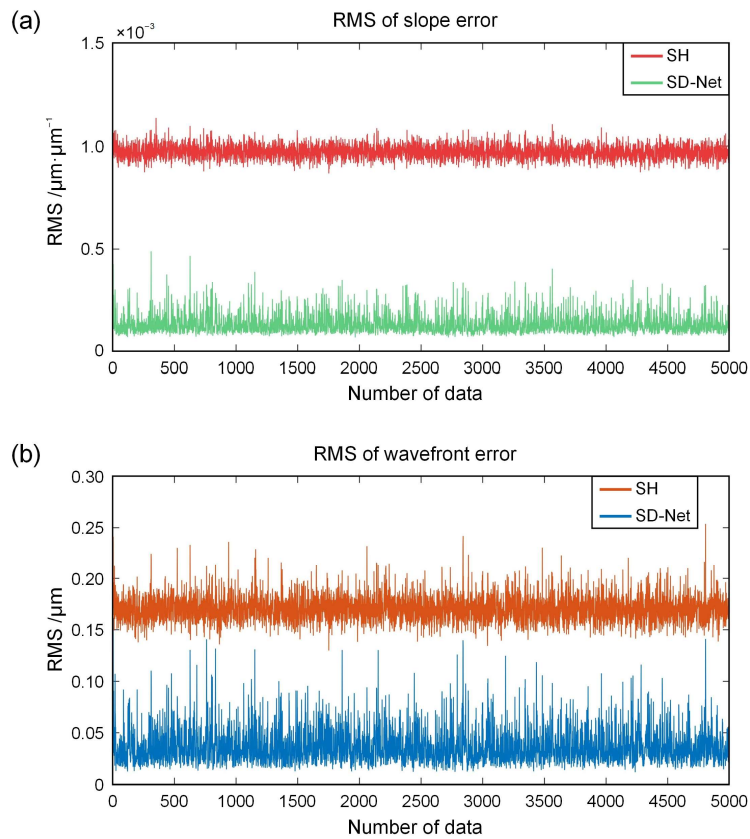

Figure 7. RMS value of reconstruction errors using DLWS and SHWFS in experiment. (a) RMS of slope reconstruction errors. (b) RMS of wavefront reconstruction errors.

The wavefront aberrations need to be corrected in real time during ignition. The AO correction performed in the experiment is used to correct the wavefront distortion shown in Figure 8. The PV value of the initial beam distortion is 1.42μm, the RMS value is 0.21μm, and the ratio of FOPAI distribution greater than $5I_{avg}$ is 5.5%. When adaptive optical correction is implemented based on a SHWFS, as shown in Figure 8(b), the laser beam profile can be controlled and the energy is distributed more evenly over the region. After the beam distortion correction based on

12

the SHWFS, the PV value and RMS value of the correction residual are 0.82μm and 0.15μm, and the ratio of FOPAI distribution greater than $5I_{avg}$ decreases to 4.1%. However, due to the limitations of the SHWFS that the ambiguity in the focus array causes the slope calculation error, the correction target is not the ideal target. The correction direction is biased, so the initial wavefront distortion cannot be fully compensated. When the system uses the wavefront measured by the DLWS for AO correction, the control signal is calculated based on the correct aberration target. The laser beam profile achieves better uniformity, and the wavefront correction residuals are smaller than the adaptive optical correction of the SHWFS, as shown in Figure 8(c). After the wavefront detection and wavefront correction using the wavefront slope correction method, the PV and RMS of the correction residual are 0.52μm and 0.08μm, and the ratio of FOPAI distribution greater than $5I_{avg}$ is 2.7%. Figure 8(d) shows the comparison of the FOPAI curve of the non-aberrated beam under the CPM, the FOPAI curve of the beam with aberration after wavefront detection and correction by the SHWFS, and the FOPAI curve of the beam with aberration after wavefront detection and correction by the DLWS. It can be seen that the wavefront detection method of the SHWFS has poor correction effect on the incident beam distortion in the CPM optical path. However, after the wavefront detection and beam distortion correction by the DLWS, the FOPAI distribution of the beam is close to the design target of the CPM, and the beam smoothing effect is better in this case. Figure 8(e) shows the comparison of key parameters of the FOPAI curve. Taking the ratios of FOPAI distribution greater than 3 times, 5 times and 7 times as the key parameters, the results show that the three ratios of the DLWS are all lower than those of the SHWFS.
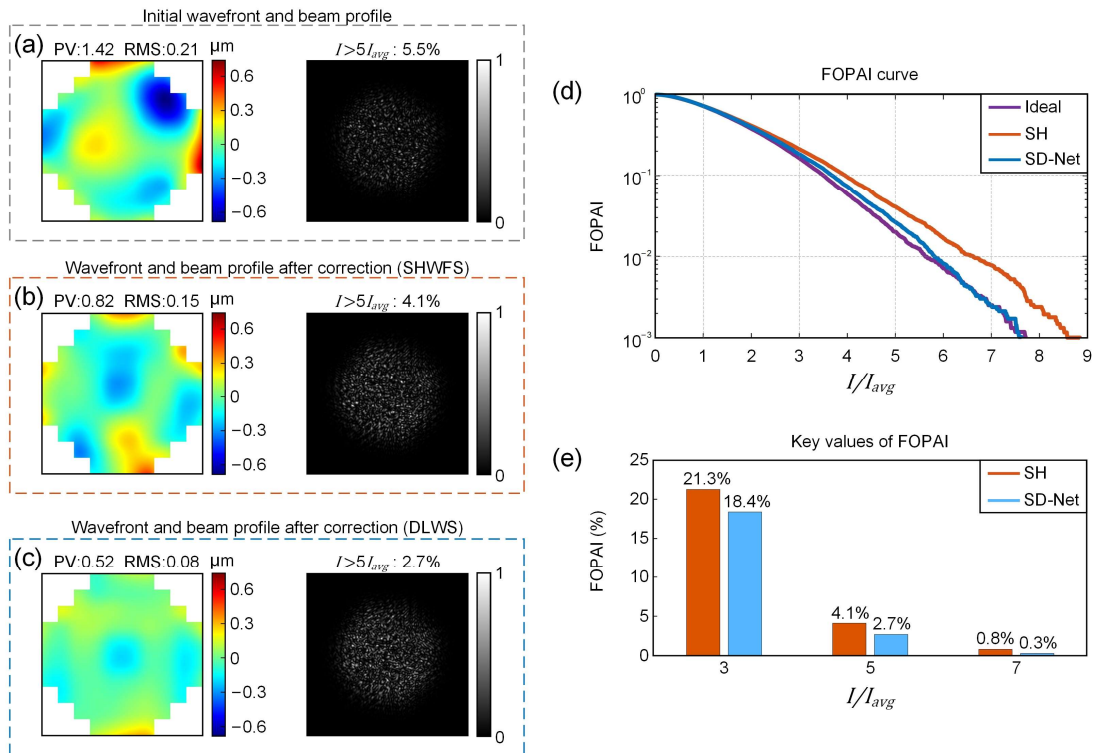
13

Figure 8. Wavefront correction results using DLWS and SHWFS. (a) Initial wavefront distortion and beam profile. (b) Wavefront reconstruction error and beam profile of SHWFS. (c) Wavefront reconstruction error and beam profile of DLWS. (d) FOPAI curves. (e) Key parameters of FOPAI.
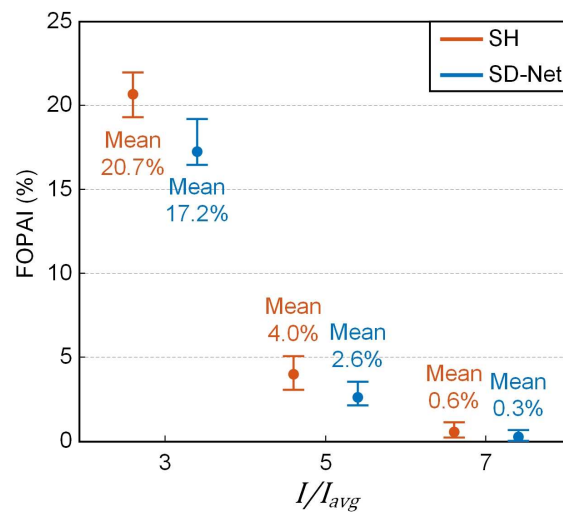

Figure 9. FOPAI results of beam profiles after wavefront correction based on the DLWS and the SHWFS.

In the experiment, 5000 sets of wavefront data were corrected and the key FOPAI data of beam intensity distribution after correction was shown in Figure 9. Similarly, the ratios of FOPAI

14

distribution greater than 3 times, 5 times and 7 times were taken as the key parameters. It can be seen that both the SHWFS and the DLWS can improve the uniformity of laser beam profile. As a passive wavefront modulator, CPM can be designed and optimized for different application scenarios, but cannot be adjusted during real-time ignition. The high power laser irradiation and sealed environment make it nearly impossible to replace the CPM for better wavefront compensation and laser beam profile. Therefore, the introduction of active wavefront correction such as AO can effectively improve the performance of CPM modulation. The AO correction based on the SHWFS and the DLWS can suppress the input optical distortion. However, when the wavefront measurement result cannot accurately represent the target to be corrected, the adaptive optical system will have deviation in the wavefront correction direction and cannot achieve the best performance. Therefore, since the DLWS has a higher wavefront reconstruction accuracy than the SHWFS, the adaptive optical correction based on the DLWS can achieve better performance, as shown in Figure 9. The ratio of FOPAI key data of laser beam profile after wavefront correction based on the DLWS is significantly lower than that of wavefront correction based on SHWFS. This shows that the introduction of the DLWS in the optical path to carry out wavefront detection and beam aberration correction can actively correct the incident beam distortion, improve the CPM modulation performance and achieve active beam smoothing, obtaining a more uniform laser intensity distribution on the focal spot.

IV. Discussion

The numerical simulation and experiment results both demonstrate that the DLWS is an effective method to correct the wavefront distortion and improve the energy uniformity in the CPM modulation process. Considering the optical system of a high power laser facility, the input wavefront distortion before the CPM process would change in real-time and would affect the beam

15

smoothing performance of the CPM as well as the spot array distortion. The distortion of each micro-lens's focus is highly characterized with the input wavefront distortion and could not be calibrated as a static system error. With the DLWS method, the input wavefront distortion could be reconstructed according to the changes of foci distortions. In terms of beam smoothing performance, the DLWS not only provides a solution of accurate wavefront measurement and active aberration correction under the CPM modulation, but also avoids the shortage of regular wavefront sensing methods that the measured wavefront could not represent the target to be corrected. With the DLWS, the wavefront characteristics of the laser beam could be obtained more precisely, offering a reliable basis for the beam correction decision. In laser fusion facilities, the SHWFS and the DM suitable for high power laser application are common devices to sense and correct the wavefront aberration of the laser beam. Moreover, the continuous phase plate (CPP), which has the same function as the CPM, is used in laser fusion facilities to achieve beam smoothing. The difference between them is that the CPP refers specifically to the phase modulating component in inertial confinement fusion systems, while the experiment of the presented CPM is carried out on an optical experimental platform. To prevent misunderstanding, the phase modulator presented in the experiment is called the CPM. Therefore, the DLWS method could be carried out in laser fusion facility given that the neural network is fine-tuned and well-trained.

Besides, in terms of real-time operation robustness, the DLWS wavefront reconstruction is based on neural network calculation which could directly get the slope information from the detector measured gray-scale map. With the SD-Net trained with good and sufficient dataset, the correction accuracy could be guaranteed. The problems that happen to traditional centroiding algorithms, such as response supersaturation or single pixel missing, would have no effect on the network calculation.

16

Moreover, in terms of adaptability, the SD-Net used in the DLWS could be adjusted according to the requirement of the application scenarios as well as the form of input and output data. For example, besides the focal spot array measured by the detector with a micro-lens array, the input of the SD-Net could be the curvature result measured by a curvature sensor or the near-field beam profile measured by a CCD. The SD-Net could directly output the wavefront instead of the slope. The high-flexibility of the network gives the DLWS high adaptability.

Finally, in terms of the effect on the original optical system, the DLWS will not change the structure of the original light path and affect the propagation of high-power laser. The DLWS uses a DM to generate wavefront training dataset and to implement AO correction. The DM is a commonly used component in laser systems with its high reflectivity and good abilities in correcting wavefront distortion in real time. The detector used in the DLWS has the same structure as the SHWFS which is also commonly used in laser systems to measure the wavefront in different laser propagation stages. The training of the SD-Net and real-time calculation run on an independent computer. In other words, the DLWS could be easily applied to the existing CPM modulation systems.

V. Conclusion

During the CPM modulation stage in laser systems, the laser beam profile is redistributed into a flat-top distribution to improve the uniformity of energy onto the focal spot and increase the energy coupling efficiency. However, when the input beam contains wavefront distortions before the CPM modulation, the modulated laser beam profile would be reshaped and the uniformity of the laser beam profile would decrease, which affects the uniform irradiation of the focal spot. The DLWS could measure the wavefront distortion accurately and implement AO correction effectively to improve the CPM modulation performance. The DLWS uses a neural network, SD-

17

Net, to accomplish slope calculation from the gray-scale map measured by a detector with a micro-lens array. Compared with the commonly used SHWFS, the DLWS could directly reconstruct the wavefront before the CPM modulation from the modulated laser beam information, leading to better AO correction results. The simulation and the experiment are carried out to investigate the performance of wavefront measurement and AO correction of the DLWS. Results indicate that using the DLWS could improve the uniformity of the laser beam profile. The DLWS has high robustness and high flexibility due to the highly adjustable neural network. In addition, the application of the DLWS does not change the structure of the original optical system.

Acknowledgement

Disclosure

Competing interests: The authors declare none.

References

1. C. Yang, H. Yan, J. Wang, and R. Zhang, "A novel design method for continuous-phase plate," Opt. Express 21, 11171–11180 (2013). DOI: https://doi.org/10.1364/OE.21.011171

2. C. Yang, R. Zhang, Q. Xu, and P. Ma, "Continuous phase plate for laser beam smoothing," Appl. Opt., 47, 1465–1469 (2008). DOI: https://doi.org/10.1364/AO.47.001465

3. S. Xu, S. Zhou, R. Wu, J. Zhang, Y. Gong, Y. Tang, and D. Liu, "Optimization of continuous phase plate for reducing near-field diffraction modulation of back-stimulated

18

Brillouin scattered light," Optik 242, 167075 (2021). DOI: https://doi.org/10.1016/j.ijleo.2021.167075

4. D. Li, N. Li, X. Su, K. Liu, P. Ji, and B. Wang, "Continuous Phase Plate Structuring by Multi-Aperture Atmospheric Pressure Plasma Processing," Micromachines 10, (2019). DOI: https://doi.org/10.3390/mi10040260

5. F. Li, Y. Gao, L. Ji, R. He, D. Liu, X. Zhao, L. Xia, W. Feng, H. Shi, D. Rao, J. Liu, Y. Cui, C. Hu, W. Ma, and Z. Sui, "Characteristics of the beam smoothing using the combination of induced spatial incoherence and continuous phase plate," Opt Lasers Eng 145, 107537 (2022). DOI: https://doi.org/10.1016/j.optlastec.2021.107537

6. C. Hu, J. Shao, C. Wei, and H. Gu, "High-precision manufacturing technology of continuous phase plate based on magnetorheological finishing," Proc. SPIE 11548, pp. 366–374 (2020). DOI: https://doi.org/10.1117/12.2573845

7. R. Zhang, H. Jia, X. Tian, H. Yuan, N. Zhu, J. Su, D. Hu, Q. Zhu, and W. Zheng, "Research of beam conditioning technologies using continuous phase plate, Multi-FM smoothing by spectral dispersion and polarization smoothing," Opt Lasers Eng 85, 38–47 (2016). DOI: https://doi.org/10.1016/j.optlaseng.2016.04.015

8. S. N. Dixit, I. M. Thomas, B. W. Woods, A. J. Morgan, M. A. Henesian, P. J. Wegner, and H. T. Powell, "Random phase plates for beam smoothing on the Nova laser," Appl. Opt. 32, 2543–2554 (1993). DOI: https://doi.org/10.1364/AO.32.002543

9. X. Jiang, J. Li, R. Wu, Z. Zhu, S. Zhou, and Z. Lin, "Performance of target irradiation in a high-power laser with a continuous phase plate and spectral dispersion," J. Opt. Soc. Am. A 30, 2162–2168 (2013). DOI: https://doi.org/10.1364/JOSAA.30.002162

10. J. Garnier, L. Videau, C. Gouédard, and A. Migus, "Statistical analysis for beam smoothing and some applications," J. Opt. Soc. Am. A 14, 1928–1937 (1997). DOI: https://doi.org/10.1364/JOSAA.14.001928

11. R. Zhang, J. Su, D. Hu, P. Li, H. Yuan, W. Zhou, Q. Yuan, Y. Wang, X. Tian, D. Xu, J. Dong, and Q. Zhu, "Research of beam smoothing technologies using CPP, SSD, and PS," Proc. SPIE 9255, p. 92554B (2015). DOI: https://doi.org/10.1117/12.2064950

12. J. Néauport, X. Ribeyre, J. Daurios, D. Valla, M. Lavergne, V. Beau, and L. Videau, "Design and optical characterization of a large continuous phase plate for Laser

19

Integration Line and laser Megajoule facilities," Appl. Opt. 42, 2377–2382 (2003). DOI: https://doi.org/10.1364/AO.42.002377

13. N. Kang, H. Liu, Y. Zhao, S. Ji, S. Zhou, and A. Lei, "Effects of continuous phase plate on plasma corona homogeneity and laser-plasma instabilities in experiments with three target materials," Plasma Phys. Control. Fusion 62, 055007 (2020). DOI: https://doi.org/10.1088/1361-6587/ab7aac

14. Y. Zhao, S.-M. Weng, H.-H. Ma, X.-J. Bai, and Z.-M. Sheng, "Mitigation of laser plasma parametric instabilities with broadband lasers," Rev. Mod. Phys. 7, 1 (2022). DOI: https://doi.org/10.1007/s41614-022-00105-0

15. O. Willi, T. Afshar‑rad, S. Coe, and A. Giulietti, "Study of instabilities in long scale‑length plasmas with and without laser‑beam‑smoothing techniques," Phys. Fluids B: Plasma Physics 2, 1318‑1324 (1990). DOI: https://doi.org/10.1063/1.859549

16. J. C. Fernández, B. S. Bauer, J. A. Cobble, D. F. DuBois, G. A. Kyrala, D. S. Montgomery, H. A. Rose, H. X. Vu, R. G. Watt, B. H. Wilde, M. D. Wilke, W. M. Wood, B. H. Failor, R. Kirkwood, and B. J. MacGowan, "Measurements of laser-plasma instability relevant to ignition hohlraums," Phys. Plasmas 4, 1849–1856 (1997). DOI: https://doi.org/10.1063/1.872328

17. I. V. Igumenshchev, W. Seka, D. H. Edgell, D. T. Michel, D. H. Froula, V. N. Goncharov, R. S. Craxton, L. Divol, R. Epstein, R. Follett, J. H. Kelly, T. Z. Kosc, A. V. Maximov, R. L. McCrory, D. D. Meyerhofer, P. Michel, J. F. Myatt, T. C. Sangster, A. Shvydky, S. Skupsky, and C. Stoeckl, "Crossed-beam energy transfer in direct-drive implosions," Phys. Plasmas 19, 056314 (2012). DOI: https://doi.org/10.1063/1.4718594

18. M. Koenig, B. Faral, J. M. Boudenne, D. Batani, A. Benuzzi, and S. Bossi, "Optical smoothing techniques for shock wave generation in laser-produced plasmas," Phys. Rev. E 50, R3314–R3317 (1994). DOI: https://doi.org/10.1103/PhysRevE.50.R3314

19. Z. Zhong, P. Hou, and B. Zhang, "Radial smoothing for improving laser-beam irradiance uniformity," Opt. Lett. 40, 5850–5853 (2015). DOI: https://doi.org/10.1364/OL.40.005850

20. V. A. Smalyuk, D. Shvarts, R. Betti, J. A. Delettrez, D. H. Edgell, V. Yu. Glebov, V. N. Goncharov, R. L. McCrory, D. D. Meyerhofer, P. B. Radha, S. P. Regan, T. C. Sangster, W. Seka, S. Skupsky, C. Stoeckl, B. Yaakobi, J. A. Frenje, C. K. Li, R. D. Petrasso, and

F. H. Séguin, "Role of Hot-Electron Preheating in the Compression of Direct-Drive Imploding Targets with Cryogenic D2 Ablators," Phys. Rev. Lett. 100, 185005 (2008). DOI: https://doi.org/10.1103/PhysRevLett.100.185005

21. A. V. Kudryashov, V. V. Samarkin, A. L. Rukosuev, and A. Alexandrov, "High-power lasers and adaptive optics," Proc. SPIE 5333, pp. 45–52 (2004). DOI: https://doi.org/10.1117/12.538450

22. A. Kudryashov, A. Lylova, V. Samarkin, J. Sheldakova, and A. Alexandrov, "Fast adaptive optical system for the high-power laser beam correction in atmosphere," Proc. SPIE 10410, p. 104100L (2017). DOI: https://doi.org/10.1117/12.2276177

23. L. Sun, Y. Guo, C. Shao, Y. Li, Y. Zheng, C. Sun, X. Wang, and L. Huang, "10.8 kW, 2.6 times diffraction limited laser based on a continuous wave Nd:YAG oscillator and an extra-cavity adaptive optics system," Opt. Lett. 43, 4160–4163 (2018). DOI: https://doi.org/10.1364/OL.43.004160

24. A. A. Aleksandrov, A. V. Kudryashov, A. L. Rukosuev, T. Yu. Cherezova, and Yu. V. Sheldakova, "An adaptive optical system for controlling laser radiation," J. Opt. Technol. 74, 550–554 (2007). DOI: https://doi.org/10.1364/JOT.74.000550

25. D. Wang, X. Zhang, Y. Yang, X. Deng, W. Dai, C. Sun, Y. Zheng, D. Hu, F. Jing, Q. Yuan, and L. Huang, "Deformable mirror resolution-matching-based two-stage wavefront sensorless adaptive optics method," Appl. Opt. 59, 6848–6860 (2020). DOI: https://doi.org/10.1364/AO.394621

26. P. Yang, Y. Liu, M. Ao, S. Hu, and B. Xu, "A wavefront sensor-less adaptive optical system for a solid-state laser," Opt Lasers Eng 46, 517–521 (2008). DOI: https://doi.org/10.1016/j.optlaseng.2008.03.003

27. H. Song, R. Fraanje, G. Schitter, H. Kroese, G. Vdovin, and M. Verhaegen, "Model-based aberration correction in a closed-loop wavefront-sensor-less adaptive optics system," Opt. Express 18, 24070–24084 (2010). DOI: https://doi.org/10.1364/OE.18.024070

28. M. Segel, A. Zepp, E. Anzuola, S. Gladysz, and K. Stein, "Optimization of wavefront-sensorless adaptive optics for horizontal laser beam propagation in a realistic turbulence environment," Proc. SPIE 10408, p. 104080E (2017). DOI: https://doi.org/10.1117/12.2276240

29. L. Gilles and B. L. Ellerbroek, "Real-time turbulence profiling with a pair of laser guide star Shack–Hartmann wavefront sensors for wide-field adaptive optics systems on large to extremely large telescopes," J. Opt. Soc. Am. A 27, A76–A83 (2010). DOI: https://doi.org/10.1364/JOSAA.27.000A76

30. A. L. Rukosuev, A. Alexandrov, V. Y. Zavalova, V. V. Samarkin, and A. V. Kudryashov, "Adaptive optical system based on bimorph mirror and Shack-Hartmann wavefront sensor," Proc. SPIE 4493, pp. 261–268 (2002). DOI: https://doi.org/10.1117/12.454721

31. Y. He, Z. Liu, Y. Ning, J. Li, X. Xu, and Z. Jiang, "Deep learning wavefront sensing method for Shack-Hartmann sensors with sparse sub-apertures," Opt. Express 29, 17669-17682 (2021). DOI: https://doi.org/10.1364/OE.427261

32. L. Hu, S. Hu, W. Gong, and K. Si, "Learning-based Shack-Hartmann wavefront sensor for high-order aberration detection," Opt. Express 27, 33504-33517 (2019). DOI: https://doi.org/10.1364/OE.27.033504

33. L. Hu, S. Hu, W. Gong, and K. Si, "Deep learning assisted Shack–Hartmann wavefront sensor for direct wavefront detection," Opt. Lett. 45, 3741-3744 (2020). DOI: https://doi.org/10.1364/OL.395579

34. W. Southwell, "Wave-front estimation from wave-front slope measurements," J. Opt. Soc. Am. 70, 998-1006 (1980). DOI: https://doi.org/10.1364/JOSA.70.000998